INVESTIGATION OF ELECTRONIC STRUCTURE AND OPTICAL PROPERTIES OF CUBIC PEROVSKITE $RbCdF_3$ FOR NOVEL APPLICATIONS

K. Ephraim Babu
Department of Physics, Narasaraopeta Engineering College(A), Narasarao Pet, Yellamanda (P.O) Guntur(D.T) Andhra Pradesh, India
Email: ephraimbabu@gmail.com

D. Deenabandhu
Department of Physics, Dr. L. B. College of Engineering for Women, Visakhapatnam.A.P.

V. Venkata Kumar
Department of BS&H, St. Ann's College of Engineering & Technology, Nayunipalli Village, ChallaReddy Palem Post, Vetapalem Mandal, Chirala, Prakasam District, AP, India

K. Bueala Kumari
Department of BS&H, St. Ann's College of Engineering & Technology, Nayunipalli Village, ChallaReddy Palem Post, Vetapalem Mandal, Chirala, Prakasam District, AP, India

K. Samatha
Department of Physics, Andhra University, Visakhapatnam, Andhra Pradesh, India

V. Veeraiah
Department of Physics, Andhra University, Visakhapatnam, Andhra Pradesh, India

Received: Jul. 2019 Accepted: Aug. 2019 Published: Sep. 2019

Abstract: The first-principles calculation is performed to investigate the energy band structure, density of states (DOS) and optical properties of cubic perovskite $RbCdF_3$ by using density functional theory (DFT) with the Local density Approximation (LDA), Generalized Gradient Approximation (GGA) and modified Becke-Johnson (mBJ) exchange potential in WIEN2K package. The ground state properties such as lattice parameter, bulk modulus and its pressure derivative are calculated and the results are compared with the available theoretical data. The contribution of the different bands was analyzed from the total and partial density of states curves. The electronic density plots reveal strong ionic bonding in Rb-F and strong covalent bonding in Cd-F. Calculations of the optical spectra, viz., the dielectric function, optical reflectivity, absorption coefficient, real part of optical conductivity, refractive index, extinction coefficient and electron energy loss, are performed for the energy range 0-30 eV.

Keywords: Density Functional Theory, Optical Properties, Electronic Structure, WIEN2K, Band Structure.

1. Introduction: Computer modelling investigation of materials has become an important tool to predict electronic, optical, magnetic and mechanical properties before one can actually synthesize the material. Now a days the synthesis and characterization of materials involve complex procedure and hence resorting to modelling studies before synthesis of the material saves time and one can have the necessary information in hand about the properties and utility of a particular material from these modelling studies. Many experimental and theoretical investigations are devoted to the study of perovskite-type flourides: typically ABF_3 (A: large cation with different valence and B: transition metal). This class of materials has great potential for a variety of device applications in optical, ferroelectric, antiferromagnetic systems [1-4] due to their wide band gaps. Moreover, wide bandgap materials are prospective candidates for vacuum-ultraviolet transparent lenses used in optical lithography steppers [5]. Crystallographic, elastic and Raman scattering investigations of structural phase transitions of $RbCdF_3$ are investigated by Rousseau et al. [6, 7]. $RbCdF_3$ has a cubic perovskite structure at room temperature and undergoes a structural phase transition at 124 K from cubic to tetragonal. When $RbCdF_3$ is doped with some transition metal ions it shows many applications in optically rewritable Bragg grating, holographic storage, passive ultra violet (UV) detection, dosimetry, and tunable laser materials [8-10]. $RbCdF_3$ is the most important perovskite fluoride crystals because they possess excellent insulator, photoluminescent, ferromagnetic and piezoelectric properties and find applications in photoelectric devices [11, 12]. The lattice constant (a) of $RbCdF_3$ has been reported to be 4.398 Å by Jiang et al.[13]. Crystal structure of $RbCdF_3$ in the cubic phase has been studied experimentally using various techniques [14,15]. Similar investigations on the first-principles study of some materials are reported in literature [16,17].

The structure of the cubic perovskites is described by the Pm-3m space group (#221). The first cation (Rb) is surrounded by 12 anions, whereas the second cation (which can be Cd) is placed at the center of an ideal octahedron formed by six anions. Fig. 1 shows a general view of the $RbCdF_3$ crystal structure (eight unit cells). To visualize the overall crystal lattice composition: it represents a three-dimensional chain of the CdF_6 octahedra, which share corners with nearest neighbours. The Rb ions are at the centers of cavities formed by the fluorine octahedra.

2. Computational Details: In this study we followed the FP-LAPW method [18] within density functional theory as implemented in the WIEN2k code [19] to calculate the required properties of the materials. This method is based on DFT [20] and has been proven to be one of the most accurate methods for computation of the electronic structure and optical properties of various solids. The exchange-correlation potential is calculated within the local density approximation [21] or generalized gradient approximation by PBE-sol [22]. The recent mBJ method [23] is also applied to calculate the electronic and optical properties of the compounds. In the FP-LAPW method, the wave function, charge density and potential are expanded by spherical harmonic functions inside non-overlapping spheres surrounding the atomic sites (muffin-tin spheres) and by a plane wave basis set in the remaining space of the unit cell (interstitial region). The Brillouin zone integration is carried out by using the

modified tetrahedron method [24]. The FP-LAPW method expands the potential in the following form:

$$V(r) = \sum_{lm} V_{lm}(r) Y_{lm}(\hat{r}) \quad \text{(inside sphere)} \qquad (1)$$

and

$$V(r) = \sum_{k} V_k e^{ikr} \quad \text{(outside sphere)} \qquad (2)$$

Where, Ylm ($\hat{r}$) is a linear combination of radial functions times spherical harmonics.

In order to achieve the energy eigenvalue convergence, we expanded the basis function up to $R_{MT} K_{max}$=7 where R_{MT} is the smallest atomic sphere radius in the unit cell and *Kmax* gives the magnitude of the largest *K* vector in the plane wave expansion. The valence wave functions inside the spheres are expanded up to *lmax*=10 while the charge density is Fourier expanded upto G_{max}=12. The sphere radii values are 2.2, 2.0 and 1.8 a.u. for Rb, Cd and F respectively. The self-consistent calculations are considered to converge when the total energy of the system is stable within 0.0001 Ry.

The dielectric function $\varepsilon(\omega) = \varepsilon_1(\omega) + i\varepsilon_2(\omega)$ is known to describe the optical response of the medium at all photon energies. The imaginary part $\varepsilon_2(\omega)$ is directly related to the electronic band structure of a material and describes the absorptive behaviour. The imaginary part of the dielectric function $\varepsilon_2(\omega)$ is given [25, 26] by

$$\varepsilon_2(\omega) = \left(\frac{4\pi^2 e^2}{m^2\omega^2}\right) \sum_{i,j} \int_k \left\langle i \middle| M \middle| j \right\rangle^2 f_i(1-f_i)\delta(E_{j,k} - E_{i,k} - \omega) d^3k \qquad (3)$$

Where, M is the dipole matrix, i and j are the initial and final states respectively, f i is the Fermi distribution function for the i-th state, and E_i is the energy of electron in the i-th state with crystal wave vector k. The real part $\varepsilon_1(\omega)$ of the dielectric function can be extracted from the imaginary part using the Kramers-Kronig relation in the form [27, 28]:

$$\varepsilon_1(\omega) = 1 + \frac{2}{\pi} P \int_0^{\infty} \frac{\omega' \varepsilon_2(\omega') d\omega'}{\omega'^2 - \omega^2} \qquad (4)$$

Where, P implies the principal value of the integral. The knowledge of both the real and imaginary parts of the dielectric tensor allows the calculation of important optical functions such as the refractive index $n(\omega)$, extinction coefficient $k(\omega)$ and reflectivity $R(\omega)$, using the following expressions:

$$n(\omega) = \left\{ \frac{\varepsilon_1(\omega)}{2} + \frac{\sqrt{\varepsilon_1(\omega)^2 + \varepsilon_2(\omega^2)}}{2} \right\}^{\frac{1}{2}} \qquad (5)$$

$$k(\omega) = \left\{ \frac{\varepsilon_1(\omega)}{2} - \frac{\sqrt{\varepsilon_1(\omega)^2 + \varepsilon_2(\omega)^2}}{2} \right\}^{\frac{1}{2}} \qquad (6)$$

$$R(\omega)=\left|\frac{\sqrt{\varepsilon(\omega)}-1}{\sqrt{\varepsilon(\omega)}+1}\right|^2 \quad (7)$$

Other optical parameters like energy loss function L(ω), absorption coefficient α(ω), and frequency dependent optical conductivity σ (ω) are calculated by the following expressions:

$$L(\omega)=\mathrm{Im}\left(-\frac{1}{\varepsilon(\omega)}\right) \quad (8)$$

$$\alpha(\omega)=\frac{4\pi k(\omega)}{\lambda} \quad (9)$$

$$\sigma(\omega)=\frac{2W_{cv}\hbar\omega}{\overrightarrow{E_0}^2} \quad (10)$$

where, Wcv is transition probability per unit time.

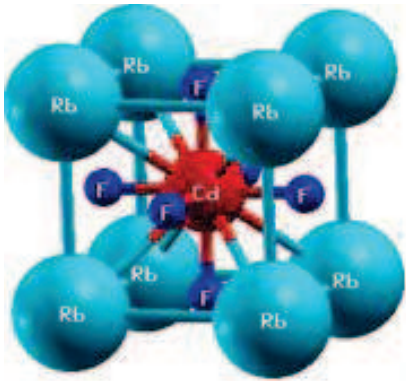

Fig.1: Crystal structures of $RbCdF_3$

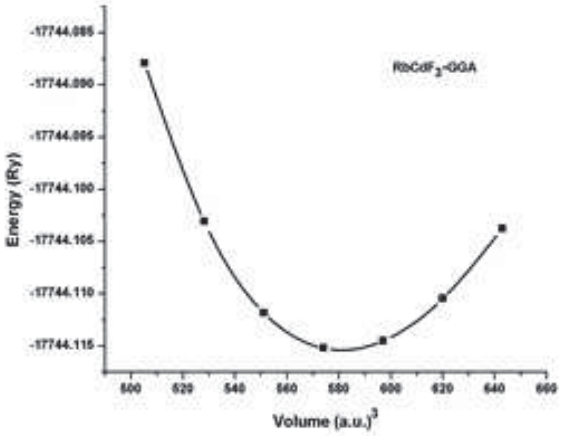

Fig. 2: Total Energy Per Unit Cell As A Function of Volume of $RbCdF_3$

Table 1: Calculated lattice constant a(Å), Bulk modulus B(GPa), Pressure derivative of Bulk modulus B′, Volume V_o (Å), Ground state energy E_o(Ry) and bond length compared with the available literature.

		Present work			
		LDA	GGA	Experiment	Other theoretical calculations
$RbCdF_3$	a (Å)	4.332	4.415	4.398	4.459[a]
	B(GPa)	75.561	67.845		62.37[a]
	B′	4.9385	4.654		
	V_0 (Å)	548.672	580.988		
	E_0(Ry)	-17734.404	-17744.115		-17754.76[a]
	Rb-F (Å)	3.063			
	Cd-F(Å)	2.163			

[a]ref.16

3. Results and Discussion:

3.1. Structural Properties: The equilibrium structural parameters are performed by fitting the total energy verses volume to the Murnaghan's equation of state [29]. Table.1 gives the calculated equilibrium lattice constant (**a**), bulk modlus (B), pressure derivative of the bulk modulus (B') and the ground state energy (E_o) within LDA and GGA approximations together with available experimental and other theoretical values. The total energy per unit cell of $RbCdF_3$ in the cubic perovskite structure is shown in Fig. 2.

3.2. Electronic Properties: The electronic properties of $RbCdF_3$ via the energy band, the total and partial density of states are presented in this section. We have applied the LDA, GGA and mBJ methods to calculate these properties. The calculated band structure for $RbCdF_3$ using LDA, GGA-PBEsol and mBJ along high symmetry directions in the first Brillion zone at equilibrium volume are given in Fig. 3. The calculated values of the band gaps are found to be equal to 3.08 eV, 3.17 eV, and 6.74 eV using LDA, GGA-PBEsol and mBJ for $RbCdF_3$ respectively. As the DFT within both LDA and GGA is known to underestimate the band gap values, the latest approach of mBJ is used to remove this discrepancy and to obtain a reliable band gap for both the compounds. The mBJ-LDA potential Vxc uses the mBJ exchange potential plus the LDA correlation potential and performs the calculations of band gap precisely. This method provides the band gaps almost equal to the experimental values [20]. The calculated energy bands along the high symmetry lines in the Brillouin zone and total as well as partial density of states of $RbCdF_3$ is shown in Fig. 3. The zero of energy is chosen to coincide with the valence band maximum (VBM), which occurs at M point, and the conduction band minimum (CBM) occurs at the Γ point resulting in an indirect band gap of 6.74 eV. The energy distributions of different states are studied by the total density of states (TDOS) while contributions of different states of the ions in different bands of the band structures are evaluated by using the partial density of states (PDOS). From Fig. 3, it is seen that the total density of states (TDOS) of the compounds can be grouped into different regions within energy range –7eV to 20 eV. The narrow band around –5 eV due to Cd *4d* states contribution is observed. From –3 eV to Fermi level, the bands have major contribution of F *2p* states and minor contribution of Cd *4d* states. There is hybridization between Cd *4d* with F *2p* states in this region. Above the Fermi level, the conduction band minimum (CBM) is composed by Cd 5*s* states for both the compounds. From 10 eV to 14 eV, majority contribution is due to Rb *4d* states. From 14 eV to 20 eV, along with Rb *4d* states a minor contribution of Cd *4f* states is observed for both the compounds.

Table 2: Calculated Band Gaps of $RbCdF_3$ along with Available Literature

	Present work			Other theoretical data
	LDA	GGA	mBJ	
$RbCdF_3$				
E_g^{R-R} (eV)	7.60	7.65	10.65	10.68[a]
$E_g^{R-\Gamma}$ (eV)	3.08	3.17	6.74	

[a]ref.16 (mBJ method)

Electron density distribution reveals the nature of chemical bonds in a material. The corresponding contour maps of the charge density distributions are shown in Fig. 4(a) along (1 0 0) plane in 2D representation, Fig.4 (b) along (1 0 0) plane in 3D representation and Fig. 4(c) along (1 1 0) plane in 2D representation. The charge distribution in the Rb cation and F anion is perfectly spherical which indicates the strong ionic nature of Rb-F bond and the charge is transferred from the Rb cation to F due to large electronegativity difference. Also the charge distribution in the Cd cation is spherical which indicates that the bonding in the CdF_6 octahedra is also purely ionic and charge is transferred from Cd to F. The bonding among the Rb and CaF_6 is also ionic, as there is no overlapping in the charge distribution among the ions. Hence, the bonding in $RbCdF_3$ compounds is purely ionic. Our theoretical results coincide with other results [16,17].

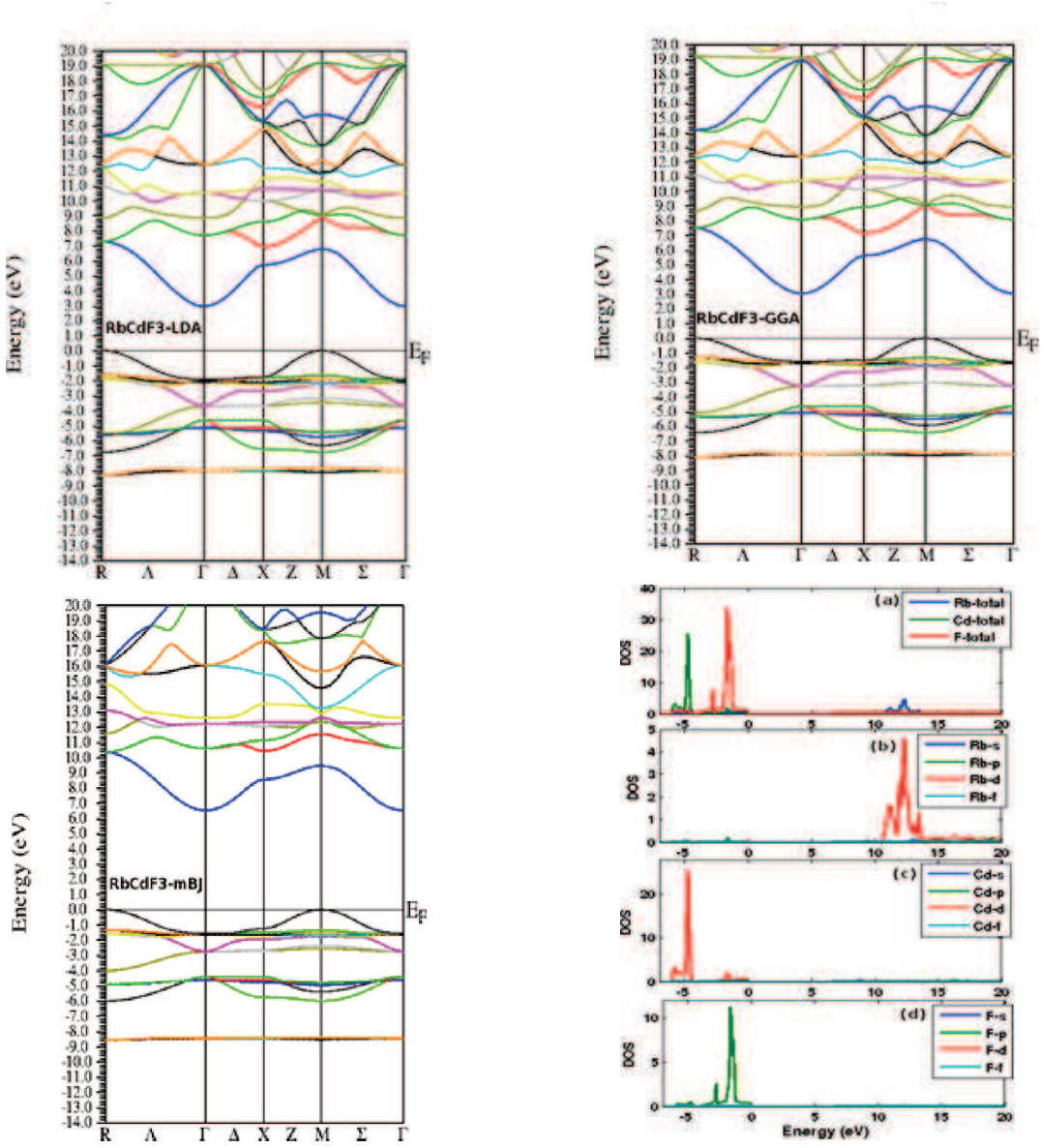

Fig. 3: Calculated Band Structure, Total and Partial Density of States of $RbCdF_3$ using LDA, GGA and mBJ Methods

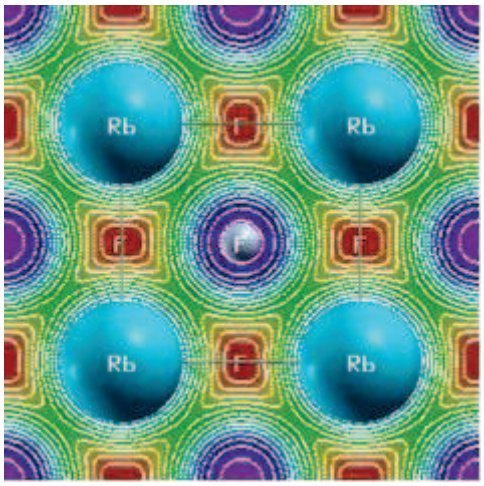

Fig. 4.(a).

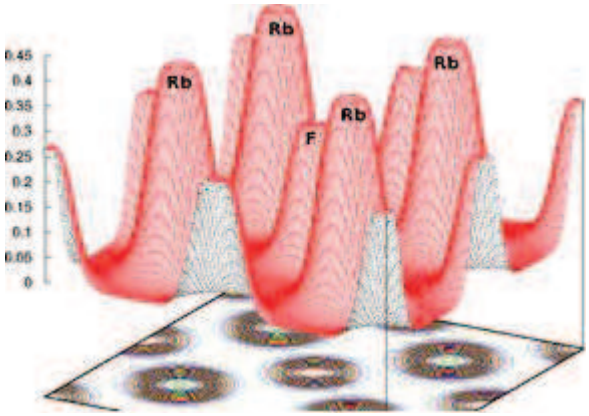

Fig. 4.(b)

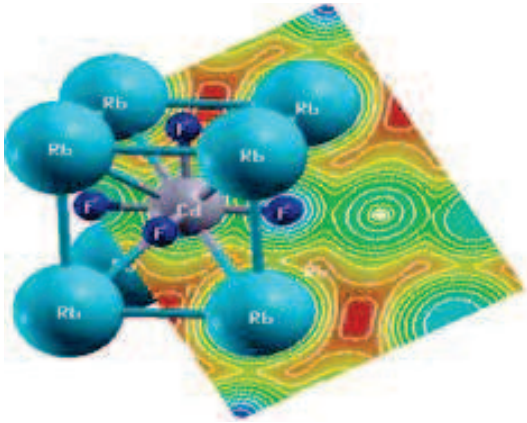

Fig. 4.(c)

Fig. 4: Charge density distribution of $RbCdF_3$ (a) along (1 0 0) plane in 2-D representation, (b) along (1 0 0) plane in 3-D representation (c) along (1 1 0) direction.

3.3. Optical Properties: We now discuss the optical properties of cubic perovskite $RbCdF_3$. The mBJ-GGA method is used to calculate the optical properties of this compound. The calculated optical properties of $RbCdF_3$ are shown in Fig. 5. The imaginary part $\varepsilon_2(\omega)$ and the real part $\varepsilon_1(\omega)$ of the dielectric function, refractive index $n(\omega)$, extinction coefficient $k(\omega)$, Reflectivity $R(\omega)$, energy loss function $L(\omega)$, optical conductivity σ (ω) and absorption coefficient $\alpha(\omega)$ of $RbCdF_3$ is shown in Fig. 5, as functions of the photon energy in the range of 0-40 eV. The imaginary part $\varepsilon_2(\omega)$ gives the information of absorption behaviour of $RbCdF_3$. In the imaginary part $\varepsilon_2(\omega)$, the threshold energy of the dielectric function occurs at $E_0 = 8.07$ eV for $RbCdF_3$. From the Fig. 5(a) for the imaginary part $\varepsilon_2(\omega)$, it is clear that there are some absorption peaks are shown in the energy range of 11.0 eV-30.0 eV. These absorption peaks can easily described by the density of states (DOS) of the compounds. In $RbCdF_3$ after the threshold points absorption of the materials increases sharply and we see different structures, which are due to the transition of electrons from Cd *4d* and F *2p* states of the valence band

(VB) to the Rb *4d* unoccupied states in the (CB) (around 10 to 14 eV). Interestingly the material shows identical spectra, except between 19.0 eV to 26.0 eV.

The real part of the dielectric function $\varepsilon_1(\omega)$ is displayed in Fig. 5(b). This function $\varepsilon_1(\omega)$ gives us information about the electronic polarizability of a material. The static dielectric constants at zero is obtained as $\varepsilon_1(0) = 1.81$ for $RbCdF_3$. From its zero frequency limit, it starts increasing and reaches the maximum value of 3.39 at 19.17 eV for $RbCdF_3$ and goes below 0 in negative scales are shown in the Table. 3. In these energy ranges the materials behave metallic while otherwise they have dielectric nature.

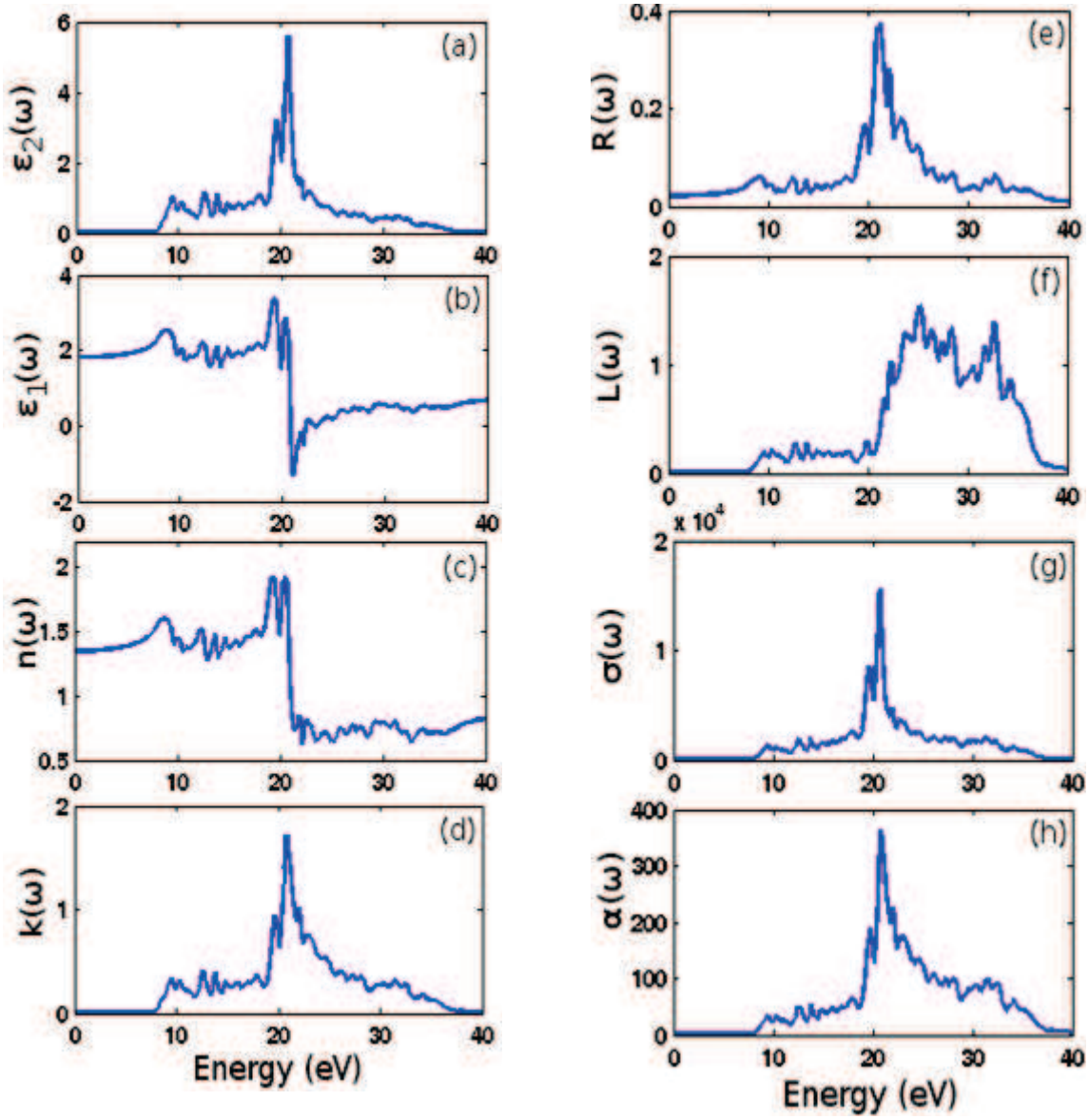

Fig. 5: Optical spectra as a function of photon energy for cubic perovskites (a) Imaginary (b) real parts of dielectric function, (c) refractive index (d) extinction coefficient (e) reflectivity (f) energy loss function (e) optical conductivity (h) absorption coefficient of $RbCdF_3$

Table 3: Calculated zero frequency limits of refractive index n(0), reflectivity R (0), energy range for $\varepsilon_1(\omega) < 0$, maximum value of refractive index n(ω), reflectivity R(ω) and optical conductivity σ (ω) of $RbCdF_3$

Present calculation	n (0)	Maximum n (ω)	Energy range (in eV) for $\varepsilon_1(\omega) < 0$	R (0) %	Maximum R (ω)	Maximum σ (ω) (in Ω^{-1} cm^{-1})
$RbCdF_3$	1.34	1.92	20.73-22.38 23.03-23.61	2.12	37.11	15592.7

The refractive index and extinction coefficient are displayed in Figs. 5(c) and 5(d). In Fig. 5(c), we observe the optically isotropic nature of this compound in the lower energy range. For lower energies, the refractive index value is almost constant and as the energy increases it attains a maximum value and exhibits decreasing tendency for higher energy values. The static refractive index n(0) are found to have the values 1.34 for $RbCdF_3$. Beyond the zero-frequency limits, it increases and reaches maximum values of 1.92 for $RbCdF_3$.

When we look at the behaviour of imaginary part of dielectric function $\varepsilon_2(\omega)$ and extinction coefficient k(ω), a similar trend is observed from Figs. 5(a) and 5(d). The extinction coefficients k(ω) reaches the maximum absorption in the medium at 20.81 eV for $RbCdF_3$. The optical reflectivity R(ω) is displayed in Fig. 5(e) and the zero-frequency reflectivity R(0) is 2.12 % for $RbCdF_3$. Beyond 9 eV, reflectivity increases and with noticeable variations it reaches to maximum value of 37.11% (21.12 eV) for $RbCdF_3$.

The energy loss function L(ω) is displayed in Fig. 5(f). This function L(ω) is an important factor describing the energy loss of a fast electron traversing in a material. The peaks in L (ω) spectra represent the characteristic associated with the plasma resonance. The resonant energy loss is seen at 25.26 eV for $RbCdF_3$. The optical conductivity σ(ω) is shown in Fig. 5(g).

The conduction of electrons due to an applied electromagnetic field is characterized by optical conductivity, σ(ω). For $RbCdF_3$, it starts from 8.13 eV and the maximum value of optical conductivity of the compound is obtained at 20.76 eV with a magnitude of 15592.7 Ω^{-1} cm^{-1}. Similar features are also observed in absorption coefficient α(ω) in the absorption range upto 40 eV and it is shown in Fig. 5(h). The imaginary part $\varepsilon_2(\omega)$ of the dielectric function is directly proportional to the absorption spectra. The maximum absorption coefficient is 362.56 m^{-1} which occurs at 20.81 eV for $RbCdF_3$. After the maximum point it again decreases at high energy with small variations. The absorption spectra indicate clearly the usefulness of this compound for absorption purposes in the ultraviolet region of the spectrum especially at around 20 to 28 eV.

4. Conclusion: In this work, we have studied first-principles calculations on the structural, electronic, elastic and optical properties for the cubic $RbCdF_3$ using the FP-LAPW method in the local density approximation (LDA), generalized gradient approximation (GGA) and the

modified Becke-Johnson potential. The ground state properties such as lattice parameter, bulk modulus and its pressure derivative are computed and compared with the available data. Much improved electronic and optical properties of $RbCdF_3$ have been calculated by using a new technique known as modified Becke Johnson (mBJ) potential. $RbCdF_3$ is an indirect band gap material (M-Γ) with a mixed ionic and covalent bonding in character. The optical properties such as dielectric function, reflectivity, absorption coefficient, real part of optical conductivity, refractive index, extinction coefficient and electron energy loss are studied in the energy range of 0-40 eV. This compound shows high absorption and reflection in the high frequency region and remain transparent in the visible region; hence it could be used for fabricating lenses and transparent coatings.

References:

1. Riadh El Ouenzerfi, Shingo Ono, Alex Quema, Masahiro Goto, Masahiro sakai et al. *J. Appl. Phys.,2004,* **96**, 7655.
2. K. Shimamura, H. Sato, A. Bensalah, V. Sudesh, H. Machida, N. Sarukura, T. Fukuda, *Cryst. Res. Technol.* , 2001, **36,** 801.
3. N. Setter, D. Damjanovis, L. Eng, G. Fox, S. Gevorgian, S. Hong, A. Kingon, H. Kohlstedt, N. Y. Park, G. B. Stephenson, I. Stolitchnov, A. K. Taganstev, D. V. Taylor, T. Yamada, S. Streiffer, *J. Appl. Phys*., 2006, **100**, 051606.
4. S.H Lim, A. C. Rastogi and S. B Desu, *J. Appl. Phys*., 2004, **96,** 5673.
5. M. Sahnoun, M. Zbiri, C. Daul, R. Khenata, H. Baltache, M. Driz., *Materials Chem. And Phy*., 2005, **91**, 185-191.
6. M. Rousseau, J. Y. Gesland, J. Julliard, J. Nouet, J. Nouet, J. Zarembowitch, A. Zarembowitch, *Phys. Rev. B*., 1975, **12**, 1579.
7. P. J. Alonso, R. Alcala, J. M. Spaeth, *Phys. Rev. B*., 1990, **41**, 10902.
8. G. V. M. Williams, C. Dotzler, A. Edgar, S. Raymond, *J Mater Sci: Mater Electron,* 2009, **20**, s268-s271.
9. C. Dotzler, G. V. M. Williams, A. Edgar, *Appl. Phys. Lett*., 2007, **91**, 181909.
10. B. Villacampa, J. Casas Gonzalez, R. Alcala, P. J. Alonso, *J. Phys,: Condens, Matter,* 1991, **3**, 8281.
11. Ai-Jie Mao and Xiao-Yu Kuang *J. Phys. Chem. A,* 2008, **112**, 2780**.**
12. J. A. Aramburu,. J. I. Paredes, M. T. Barriuso, M. Moreno, *Phys. Rev. B,* 2000, **61**, 6525.
13. L.Q. Jianga, J.K. Guod, H.B. Liua, M. Zhua, X. Zhoua, P. Wuc, C.H. Lia, A. *J. Phys. And Che. Solids*, 2006, **67**, 1531
14. O. Muller, R. Roy, The major Ternary Structural Families, Springer, New York-Heidelberg-Berlin, 1974
15. A. S. Verma, V. K. Jindal, *J. Alloys Compd*. 2009, **485**, 514.
16. G. Murtaza, Hayatullah, R. Khenata, M. N. Khalid, S. Naeem, *Physica B*, 2013, **410**, 131-136
17. K. Ephraim Babu, N. Murali, K. Vijaya Babu, B. Kishore Babu, V. Veeraiah, *Chin Phys Lett.*, 2015, **32**, 016201.
18. P. Blaha, K. Schwarz, P. Sorantin, S. B. Trickey, *Comput. Phys. Commun*., 1990, **59**, 399

19. P. Blaha, K. Schwarz, G. K. H. Madsen, D. Kvasnicka, and J. Luitz, in WIEN2K: An Augmented Plane Wave Plus Local Orbitals Program for Calculating Crystal Properties, Ed. by K. Schwarz (Vienna Technological University, Vienna, Austria, 2001).
20. W. Kohn, L.J. Sham, *Phys. Rev.B,* 1965, **140**, 1133
21. J. R. Perdew, Y. Wang, *Phys. Rev. B,* 1992, **45**, 13244.
22. J.P. Perdew, A. Ruzsinszky, G.I. Csonka, O.A. Vydrov, G.E. Scuseria, *Phys. Rev. Lett.*, 2008, **101**, 239702.
23. F. Tran, P. Blaha, *Phys. Rev. Lett*., 2009, **102**, 226401.
24. P.E. Blochl, O. Jepsen, O.K. Anderson, *Phys. Rev. B,* 1994, **49**, 16223.
25. N.V. Smith, *Phys. Rev. B,* 1971, **3**, 1862.
26. C. Ambrosch-Draxl, J.O. Sofo, Comput. Phys. Commun., 2006, **175**, 1.
27. M. Fox, Optical Properties of Solids, (*Oxford University Press, New York*, 2001).
28. F. Wooten, *Optical properties of Solids*, (Acadmic Press, New York, 1972).
29. F. D. Murnaghan, Proc. Ntal. Acad. Sci. USA, 1944 **30**, 244.

***